Indications of strong neutral impurity scattering in $Ba(Sn,Sb)O_3$ single crystals

Hyung Joon Kim,[1] Jiyeon Kim,[2] Tai Hoon Kim,[1] Woong-Jhae Lee,[1] Byung-Gu Jeon,[1] Ju-Young Park,[1] Woo Seok Choi,[3,4] Da Woon Jeong,[3,4] Suk Ho Lee,[5] Jaejun Yu,[2] Tae Won Noh,[3,4] and Kee Hoon Kim[1,*]

[1]*Center for Novel States of Complex Materials Research, Department of Physics and Astronomy, Seoul National University, Seoul 151-747, South Korea*

[2]*Center for Strongly Correlated Materials Research, Department of Physics and Astronomy, Seoul National University, Seoul 151-747, South Korea*

[3]*Center for Functional Interfaces of Correlated Electrons Systems, Institute for Basic Science (IBS), Seoul 151-747, South Korea*

[4]*Department of Physics & Astronomy, Seoul National University, Seoul 151-747, South Korea*

[5]*Southwestern Research Institute of Green Energy Technology Foundation, Mokpo 530-831, South Korea*

(Received 4 February 2013; revised manuscript received 13 May 2013; published 10 September 2013)

It was recently discovered that a transparent *n*-type $(Ba,La)SnO_3$ system has electrical mobility as high as 320 $cm^2\ V^{-1}\ s^{-1}$ at room temperature and superior thermal stability up to ~500 °C. To understand comparatively the carrier-scattering mechanism in the doped $BaSnO_3$, we investigate the physical properties of the single crystals of $BaSn_{1-x}Sb_xO_3$ ($x = 0.03$, 0.05, and 0.10), which also show the *n*-type characters via the Sn site doping by Sb. Transmittance of the grown single crystals in the visible spectral region turn out to be similar to that of the $(Ba,La)SnO_3$ system, maintaining optical transparency. Temperature-dependent Hall effect measurements reveal that the electrical mobility at room temperature reaches as high as 79.4 $cm^2\ V^{-1}\ s^{-1}$ at a carrier density of $1.02 \times 10^{20}\ cm^{-3}$, and upon increasing carrier density further, it systematically decreases nearly proportional to the inverse of the carrier density. The overall reduced mobility of the $Ba(Sn,Sb)O_3$ system as compared to the $(Ba,La)SnO_3$ system is attributed to the enhanced scattering caused by the Sb ions located in the direct conduction path. Based on the inverse proportionality between the carrier density and the electrical mobility, we suggest that the neutral impurity scattering becomes particularly strong in the $Ba(Sn,Sb)O_3$.

DOI: 10.1103/PhysRevB.88.125204 PACS number(s): 81.05.Hd, 71.20.Nr, 72.10.Bg, 72.20.Dp

I. INTRODUCTION

During the last decade, transparent conducting oxides (TCOs) and transparent oxide semiconductors (TOSs) have received increasing attention due to the enormous demand in display industries. Numerous wide band gap oxide semiconductors, including ZnO, In_2O_3, and SnO_2, have been investigated for these purposes, successfully demonstrating transparent conducting windows as well as semiconducting devices such as *pn* junctions, field effect transistors, and ultraviolet lasers.[1–8] However, those well-known material systems still have their own limitations, so active scientific researches are currently underway to find alternative transparent materials that can potentially exhibit better physical properties, e.g., high mobility for developing transparent logic devices with a fast operation speed and oxygen stability to overcome interface degradation problems in the oxide *pn* junctions.

In the past few years, various perovskite structures have also been tested as candidate materials for new TCOs and TOSs such as doped $SrTiO_3$, and $CaTiO_3$ (see Refs. 9–11). Although alkaline earth stannates with the general formula $ASnO_3$ (A = Ba, Sr, and Ca) have been widely used in several applications such as photovoltaic and/or photochemical energy conversions, stable capacitors, and gas sensors,[12–14] it is in very recent findings that the La-doped $BaSnO_3$, i.e., $(Ba,La)SnO_3$, can become highly mobile *n*-type semiconductors. $BaSnO_3$ has a cubic perovskite structure [Fig. 1(a)] and corresponds to a transparent, wide band gap semiconductor with an optical gap of more than 3.1 eV.[15] In order to induce the electrical conductivity in this material, it has been known from the studies of polycrystalline samples and thin films that both the Ba and Sn sites can be doped by La and Sb, respectively, to form $Ba(Sn,Sb)O_3$ and $(Ba,La)SnO_3$.[16–21] However, to understand their intrinsic transport properties, studies of single crystalline samples become essential because the polycrystalline and thin-film specimens can be severely subject to the large extra-scattering from grain boundaries and dislocations.

It was recently reported that high quality single crystals of $(Ba,La)SnO_3$ can be grown by the Cu_2O flux, exhibiting the room temperature mobility as high as ~300 $cm^2\ V^{-1}\ s^{-1}$ while maintaining its optical transparency.[22,23] It is noteworthy that another study on the $(Ba,La)SnO_3$ single crystals grown by the PbO-based flux reported a maximum mobility of 103 $cm^2\ V^{-1}\ s^{-1}$, which is a bit lower than 300 $cm^2\ V^{-1}\ s^{-1}$ possibly due to the effect of Pb impurities inside the crystals.[24] Related to this result and for further applications, it seems quite necessary to understand the intrinsic and extrinsic scattering mechanisms in the perovskite stannates.

In this article, we report successful growth of $Ba(Sn,Sb)O_3$ single crystals by the Cu_2O flux and discuss the intrinsic transport properties in comparison with $(Ba,La)SnO_3$. We found that $Ba(Sn,Sb)O_3$ single crystals have high optical transmittance in a visible spectral region, similar to $(Ba,La)SnO_3$, and exhibit a high electrical mobility of 79.4 $cm^2\ V^{-1}\ s^{-1}$ at room temperature at a carrier density $1.02 \times 10^{20}\ cm^{-3}$. The observed mobility is higher than those of other reported Ti-based perovskite oxides such as $SrTiO_3$ (~11 $cm^2\ V^{-1}\ s^{-1}$), $BaTiO_3$ (~2 $cm^2\ V^{-1}\ s^{-1}$), and $CaTiO_3$ (~8 $cm^2\ V^{-1}\ s^{-1}$) at room temperature.[25–27] However, the mobility of $Ba(Sn,Sb)O_3$ is obviously smaller than the reported high values of $(Ba,La)SnO_3$ (200–300 $cm^2\ V^{-1}\ s^{-1}$). In order to understand such reduced mobility in the Sn-site doped

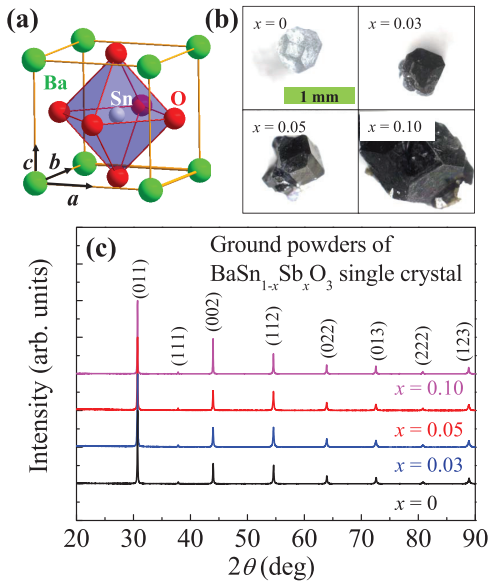

FIG. 1. (Color online) (a) Unit cell of cubic perovskite $BaSnO_3$. (b) Optical microscope images of the flux grown $BaSnO_3$ and $Ba(Sn,Sb)O_3$. (c) X-ray θ-2θ scan patterns of $BaSn_{1-x}Sb_xO_3$ single crystals.

$Ba(Sn,Sb)O_3$, we investigate doping-dependent mobility behaviors and the first-principles calculations.

II. EXPERIMENTS

For the single crystal growth of $BaSn_{1-x}Sb_xO_3$ ($x = 0$, 0.03, 0.05, and 0.1), the polycrystalline specimens with the same nominal doping levels were first synthesized to be used as a seed material in the molten flux. The polycrystalline $Ba(Sn,Sb)O_3$ specimens were prepared by the solid-state reaction method with high purity $BaCO_3$, SnO_2, and Sb_2O_3 powders. After being weighed in a stoichiometric ratio, the well-mixed powders were pressed into a pellet and calcined at 1250 °C for 6 hours. After several intermediate grindings, the pellet was finally sintered at 1400–1450 °C for 24–48 hours. For the growth of $Ba(Sn,Sb)O_3$ single crystals, a mixture of Cu_2O flux and the sintered powder with a molar ratio of about 1:15 was put into a Pt crucible, fired in air above 1250 °C, and then slowly cooled down to 1210 °C, followed by a slow furnace cooling to room temperature. The grown crystals show a cubelike shape or a truncated octahedron shape, as shown in Fig. 1(b). We investigated the structural properties of the poly- and single-crystalline samples by x-ray diffraction (XRD), for which we used a high power x-ray diffractometer equipped with a single Cu $K_{\alpha 1}$ source (Empyrean^{TM}, PANalytical).

We performed the first-principles density functional theory calculations by using of the Vienna *Ab initio* Simulation Package code.[28] We employed the projector-augmented wave method[29] and the Ceperley-Alder parameterization within the local density approximation (LDA).[30] To determine the electronic structure of $Ba(Sn,Sb)O_3$, we adopted a $3 \times 3 \times 3$ supercell containing 135 atoms and carried out the k-space integration using a $2 \times 2 \times 2$ mesh within the Monkhorst-Pack k-point sampling. All atomic coordinates were relaxed for the calculation and the Hellmann-Feynman force reached below 0.02 eV Å^{-1}. An energy cut-off for the plane wave basis set was 520 eV.

Temperature-dependent resistivity was measured by the conventional four-probe technique from 2 to 300 K either in a closed-cycle refrigerator or in a physical property measurement system (PPMS^{TM}, Quantum Design). The five-wire configuration was employed to investigate the Hall effect in single crystals as a function of temperatures in a magnetic field up to nine tesla. To make electrical contacts, the single crystals were cut and polished into a rectangular plate shape ($\sim 1 \times 0.5 \times 0.05$ mm^3). The gold film, 100-nm-thick, was subsequently deposited on the top of the polished crystal surface in a small rectangular shape by use of a shadow mask, and four rectangular pads, each of which has the typical size of 0.05×0.05 mm^2, were deposited for the longitudinal (resistivity) and transverse (Hall effect) voltage measurements. Two line pads were also deposited at both ends of the specimen for the current pads.

Optical transmission spectra were obtained in the optically polished $Ba(Sn,Sb)O_3$ single crystals, of which the thicknesses were less than 100 μm. The ultraviolet-to-visible-to-near infrared transmission spectra were measured by using a fiber-optic spectrometer (StellaNet, EPP2000) and a Xe-arc lamp as a light source. For calculating the absorption coefficient (α), we repeated the transmission measurements of the same piece of the sample in two different thicknesses and used the formula $\alpha = -\ln(T_{thick}/T_{thin})/d$, where d is the difference in thickness.

III. RESULTS

A. Structural characterization and chemical analyses

Figure 1(c) shows the powder XRD patterns (θ-2θ scan) of the $Ba(Sn,Sb)O_3$ single crystals after being grounded into fine powders. The patterns reveal that the single crystal forms in a cubic perovskite structure without any impurity phase within the detection limit. Figure 2(a) shows the Rietveld refinement result for the ground powders of the $BaSn_{0.97}Sb_{0.03}O_3$ single crystal. The lattice constant a obtained by fitting was 4.1179(8) Å with the R factor of 17.5. Figure 2(b) compares the variation of the lattice constant a as a function of x for poly- and single-crystalline $BaSn_{1-x}Sb_xO_3$ ($x = 0.00$–0.20), as obtained from the refinement. For both poly and single crystals, a is found to increase overall with increasing Sb concentration. Such lattice expansion with the Sb doping was also observed in previous experimental studies on the polycrystalline $Ba(Sn,Sb)O_3$.[16,18] It is noted in Fig. 2(b) that the increment of the lattice constant is smaller for single crystals compared to those of polycrystalline samples with the same nominal doping. This observation indicates that the actual Sb doping in the single crystals should be less than the doping levels in the polycrystals, which might be related to the formation of the other competing phases such as $BaSb_2O_6$ and $CuSb_2O_6$ inside the molten flux. If the lattice constant of the polycrystalline samples directly reflects the intrinsic doping levels, the estimated concentrations (x_e) of $BaSn_{1-x}Sb_xO_3$ single crystals with nominal $x = 0.03$, 0.05, and 0.10 become $x_e = 0.0148$, 0.0183, and 0.0240, respectively.

To find actual Sb-doping levels, we also perfomed the electron-probe microanalyses (EPMA) study of our

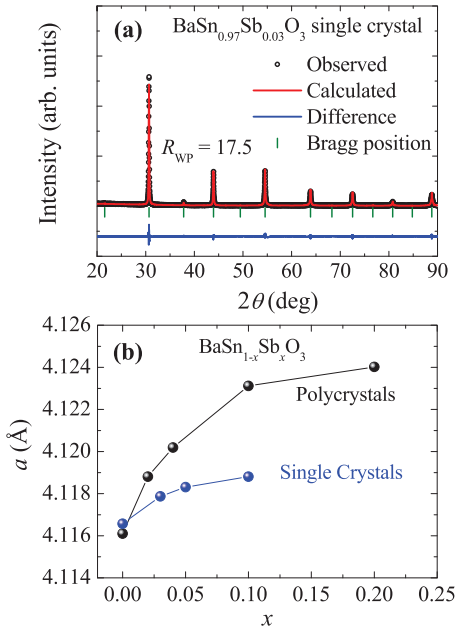

FIG. 2. (Color online) (a) Observed (open circle) and calculated (line) powder XRD patterns for the $BaSn_{0.97}Sb_{0.03}O_3$ single crystal at room temperature. The blue line shows the difference between the observed and calculated diffraction patterns. (b) Cubic lattice constant a for polycrystalline (black) and single crystalline (blue) $BaSn_{1-x}Sb_xO_3$ as a function of x.

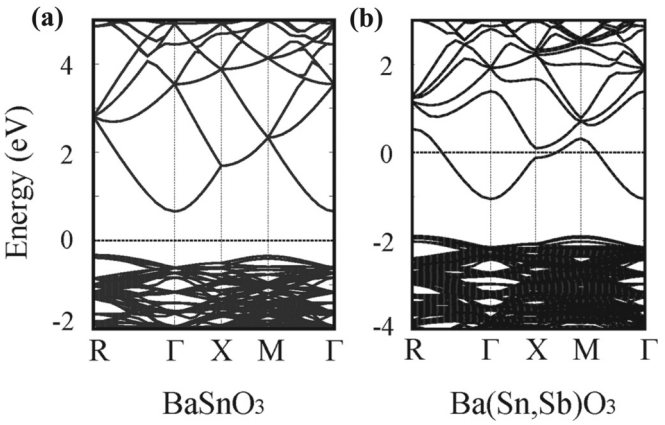

FIG. 3. The band structure of (a) $BaSnO_3$ and (b) $Ba(Sn,Sb)O_3$ obtained by first-principles calculations with 27 ($3 \times 3 \times 3$) unit cells. For $BaSn_{1-x}Sb_xO_3$, one of the Sn ions is substituted by a Sb ion corresponding to the doping rate of $x = 0.037$.

$Ba(Sn,Sb)O_3$ and $(Ba,La)SnO_3$ single crystals with polycrystalline samples as references. We observed seven points in each samples. Table I summarizes the EPMA results. In both $Ba(Sn,Sb)O_3$ and $(Ba,La)SnO_3$ systems, the ratios of (Ba + La):Sn:O and Ba:(Sn + Sb):O are almost 1:1:3, which indicates that Ba or Sn vacancies, if any, are quite small and almost similar in both systems. According to Table I, the La-doping levels in $(Ba,La)SnO_3$, are found to be almost similar to the nominal doping level. However, in the case of $Ba(Sn,Sb)O_3$, it is obvious that the Sb-doping levels are much lower than the nominal doping levels. The actual Sb doping levels determined from the EPMA results for $BaSn_{0.95}Sb_{0.05}O_3$ and $BaSn_{0.9}Sb_{0.1}O_3$ single crystals become $x_e = 0.0143$ and 0.0221, respectively, which turn out to be almost consistent with the estimated doping levels from the lattice constants of polycrystals.

Based on the smaller ionic radius of Sb^{5+} ($r = 0.060$ nm) rather than Sn^{4+} ($r = 0.069$ nm) and the lattice expansion by Sb doping, one might argue that Sb inside the crystals remain as Sb^{3+} ($r = 0.072$ nm). If the valence state of Sb is 3 +, however, the $Ba(Sn,Sb)O_3$ should become p-type semiconductors. On the other hand, the Hall effect measurements show that the $Ba(Sn,Sb)O_3$ system has the n-type carriers, which is suggestive of Sb^{5+}. Therefore, the lattice expansion cannot be simply understood in terms of a mere consideration of the ionic radii. We will further discuss this issue in the physical interpretation of first-principles calculations of $Ba(Sn,Sb)O_3$ in the following section.

B. First-principles calculations

Figures 3(a) and 3(b) show the band structures of both $BaSnO_3$ and $Ba(Sn,Sb)O_3$, respectively, as obtained by first-principles calculations with LDA. The band structures of $BaSnO_3$ and $Ba(Sn,Sb)O_3$ were drawn for the $3 \times 3 \times 3$ (unit) super-cell with 27 unit cells corresponding to $BaSn_{0.963}Sb_{0.037}O_3$. The highly dispersive conduction band of $BaSnO_3$ [Fig. 3(a)] is mainly composed of Sn 5s states with Sn-O antibonding character. According to the folded Brillouin zone in Fig. 3(b), the Sb doping gives rise to the electronic states directly into the conduction band; thus, the Fermi level forms well inside the Sn 5s band [the dotted line in Fig. 3(b)]. The electronic states in the band of the antibonding character is likely to result in repulsive forces between Sn and O to lower the total energy of the crystal structure, thereby inducing the lattice expansion as seen in Fig. 2(b). The theoretical equilibrium lattice constants of $BaSnO_3$ and Sb-doped $BaSnO_3$ by 3.7% are found to be 4.098 Å and 4.112 Å, respectively, clearly showing the increasing trend upon Sb doping to be consistent with the experimental results.

TABLE I. Chemical compositions of $(Ba,La)SnO_3$ and $Ba(Sn,Sb)O_3$ single crystals

	Composition (mol%)				Doping level (x)	
	Ba	Sn	Dopant (La or Sb)	O	EPMA	XRD refinement
$Ba_{0.99}La_{0.01}SnO_3$	20.64 ± 0.37	19.93 ± 0.30	0.217 ± 0.04	59.21 ± 0.40	0.0104	–
$Ba_{0.98}La_{0.02}SnO_3$	20.47 ± 0.53	19.88 ± 0.35	0.490 ± 0.04	59.16 ± 0.70	0.0233	–
$BaSn_{0.95}Sb_{0.05}O_3$	20.48 ± 0.20	19.64 ± 0.40	0.285 ± 0.02	61.17 ± 0.33	0.0143	0.0183
$BaSn_{0.9}Sb_{0.1}O_3$	20.64 ± 0.55	19.30 ± 0.45	0.436 ± 0.03	59.62 ± 0.45	0.0221	0.0240

Other than a small hybridization gap development near the Fermi level at the X point, the change of the band structure by the Sb doping is overall negligible, thus maintaining the dispersive conduction band of $BaSnO_3$. The calculated effective mass (m^*) of $Ba(Sn,Sb)O_3$ based on the LDA is $\sim 0.40 m_0$, where m_0 is the free-electron mass. The calculated effective mass is indeed comparable to those of other well-known TOSs such as In_2O_3 ($0.30 m_0$),[31] SnO_2 ($0.38 m_0$),[32] and ZnO ($0.24 m_0$).[33] However, the value is clearly smaller than those of Ti-based pevrovskite oxides such as $BaTiO_3$ ($5.3 m_0$), $CaTiO_3$ ($4.0 m_0$), and $SrTiO_3$ ($4.8 m_0$),[34] suggesting that the $BaSnO_3$ can become another mother compound in developing TCOs/TOSs with a high electrical mobility. It is also worth mentioning that the recently predicted effective mass of $BaSnO_3$ becomes even smaller, i.e., $0.06 m_0$ (Ref. 35) and $0.20 m_0$ (Ref. 36), which were obtained by the generalized gradient approximation or a specific hybrid-functional method, respectively. This implies that the predicted effective mass is rather sensitive to the approximation method in the calculation. Therefore, it would be necessary to determine the effective mass of the doped $BaSnO_3$ experimentally.

C. Transport properties

Figure 4 shows the plot of resistivity and mobility vs. carrier density at room temperature in $BaSnO_3$, $Ba(Sn,Sb)O_3$, and $(Ba,La)SnO_3$ single crystals.[22,23] The nominally undoped $BaSnO_3$ turns out to show the n-type carriers, which are presumably introduced by the oxygen vacancies created during the crystal growth procedure at high temperatures under air conditions. Assuming the measured carrier density of

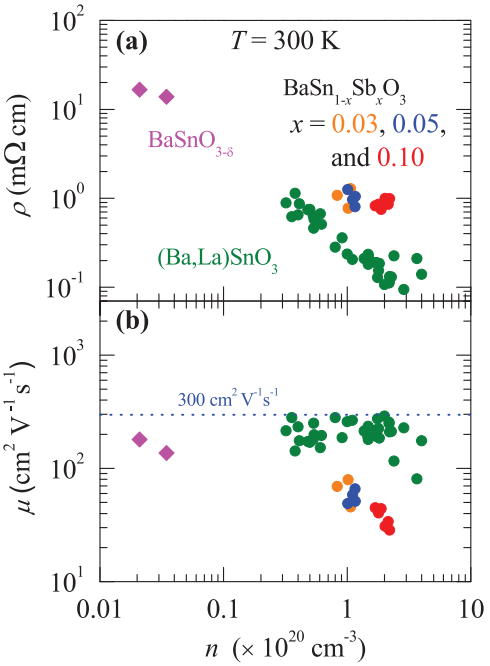

FIG. 4. (Color online) (a) Resistivity (ρ) and (b) mobility (μ) vs. carrier density (n) plot. Closed green circles are the reported data of $(Ba,La)SnO_3$ single crystals.[22,23] Closed orange, blue, and red circles represent the $BaSn_{1-x}Sb_xO_3$ single crystals with $x = 0.03$, 0.05, and 0.10, respectively. Closed violet diamonds represent the undoped $BaSnO_{3-\delta}$ single crystals.

$BaSnO_{3-\delta}$ single crystals ($\sim 2.0-3.0 \times 10^{18}$ cm^{-3}) and the fact that one oxygen vacancy gives two electron carriers, the density of oxygen vacancies is estimated to be $\sim 1.0-1.5 \times 10^{18}$ cm^{-3}.

$Ba(Sn,Sb)O_3$ single crystals also show the n-type carriers according to the Hall effect results. One noticeable feature is that the measured carrier densities of $Ba(Sn,Sb)O_3$ single crystals are even smaller than the actual doping levels, which is estimated by the lattice constants of the single crystals in comparison to those of polycrystals. If only a purely Sb^{5+} valence state is allowed to give rise to one electron to the conduction channel, the estimated doping levels of $x_e = 0.0148$, 0.0183, and 0.0240 for the three kinds of crystals [Fig. 2(b)], should create the carrier density of 2.10×10^{20} cm^{-3}, 2.60×10^{20} cm^{-3}, and 3.41×10^{20} cm^{-3}, respectively. However, the measured carrier densities are only about half of the calculated values, i.e., 9.71×10^{19} cm^{-3} ($x_e = 0.0148$), 1.09×10^{20} cm^{-3} ($x_e = 0.0183$), and 1.93×10^{20} cm^{-3} ($x_e = 0.0240$). This observation suggests that the Sb dopant can induce only half of the expected free electrons, with the other half remaining inactive. In other words, nearly half of the expected free carriers are likely to be trapped or localized. If one electron is trapped near Sb^{5+}, the bound state of $Sb^{5+} + e^-$ would be effectively similar to Sn^{4+} so that it might act as a neutral impurity in the system. If the two electrons are trapped, then the effective valence should look like $3+$.

In an earlier polycrystalline $Ba(Sn,Sb)O_3$ study, a relatively high resistivity was attributed to the carrier-trapping effect, possibly induced by a microscopic charge disproportion into Sb^{3+} and Sb^{5+} (see Ref. 16). However, earlier Mössbauer and the x-ray photoemission spectroscopy (XPS) studies observed only a single resonant absorption peak and a single Sb $3d_{3/2}$ binding energy, respectively, supporting that the valence state of Sb is close to the single Sb^{5+} state without having the Sb^{3+} state.[17] Recently, another XPS study reported that the binding energy of the Sb $3d_{3/2}$ core level shifts to a lower energy with an increase of the Sb concentration. This observation was interpreted as the tendency of mixed states of Sb^{5+} and $Sb^{5+} + e^-$ (Sb^{4+}-like) in $Ba(Sn,Sb)O_3$ (see Ref. 18). If $Ba(Sn,Sb)O_3$ is similar to the conventional semiconductors such as Si where a covalent bonding is dominant, it is expected that the hydrogenlike boundstate, $Sb^{5+} + e^-$, can become easily unstable at room temperature. However, if the boding character is close to be ionic in $Ba(Sn,Sb)O_3$, it is a plausible scenario that the Sb ions can exhibit mixed-valent characters to mitigate the Coulomb energy.

Yet another possible mechanism for inducing reduced carrier activation could be the formation of interstitial oxygen or cation vacancy. Both of these vacancy types can in principle act like neutral impurities, which would then naturally reduce the carrier activation and increase the neutral impurity scattering. In the case of Sn-doped In_2O_3, it was reported that significant decreases in carrier activation and electrical mobility occur due to the presence of interstitial oxygens and related Sn-O defect-complexes.[37] If such interstitial oxygens are present in the $Ba(Sn,Sb)O_3$ crystals, it is similarly expected that the defect complex made of Sb and interstitial oxygen can be formed to act like neutral impurities. On the other hand,

it is known in $BaTiO_3$ that a cation vacancy can be more easily formed than the interstitial oxgen.[38] However, a recent theoretical study[39] revealed that in the case of $BaSnO_3$, the formation energy of an interstitial oxygen is clearly lower than that of a cation vacancy. Therefore, the defect complexes made of Sb and interstitial oxygen can considered as the next probable candidate for causing strong neutral impurity scattering in $Ba(Sn,Sb)O_3$.

In Figs. 4(a) and 4(b), it is noted that the highest mobility of $Ba(Sn,Sb)O_3$ at room temperature is found to be 79.4 $cm^2 V^{-1} s^{-1}$ at a carrier density of 1.02×10^{20} cm^{-3}. However, the maximum mobility of $Ba(Sn,Sb)O_3$ is smaller than that of $(Ba,La)SnO_3$ (see Refs. 22 and 23) at a similar carrier density, resulting in a higher room temperature resistivity in Fig. 4(a). The lower mobility in the former system directly reflects that the Sb dopants become stronger scattering sources than the La dopants. In Fig. 4(b), the mobility of $Ba(Sn,Sb)O_3$ is rapidly reduced as the carrier density increases, while that of $(Ba,La)SnO_3$ is almost independent of carrier density. The main differences between $Ba(Sn,Sb)O_3$ and $(Ba,La)SnO_3$ are the dopant species and the location of dopants, i.e., Sb for Sn site and La for Ba site. In Sec. IV, we will discuss the origin of the contrasting carrier density vs. mobility behaviors based on the various scattering mechanisms.

The temperature-dependence of the transport properties of the $BaSnO_{3-\delta}$ and $Ba(Sn,Sb)O_3$ single crystals is shown in Fig. 5. All the measured carrier densities are found to be almost temperature-independent [Fig. 5(a)], and the resistivity exhibits mostly metallic behavior [Fig. 5(b)], indicating that the crystals are in a degenerately doped regime. The slightly increasing behavior observed in the resistivity of the $BaSnO_{3-\delta}$ single crystal at low temperatures indicates that electron

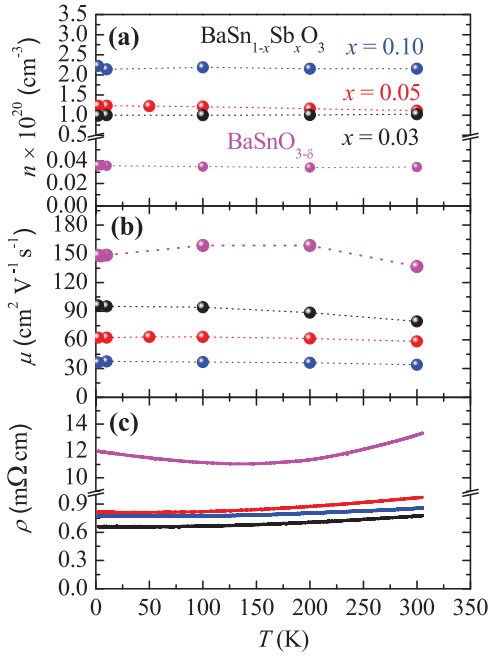

FIG. 5. (Color online) (a) Temperature-dependent carrier density, n; (b) mobility, μ; and (c) resistivity, ρ are plotted for selected $BaSnO_{3-\delta}$ (violet) and $BaSn_{1-x}Sb_xO_3$ single crystals with $x = 0.03$ (black), 0.05 (red), and 0.10 (blue).

carriers introduced by oxygen vacancies are localized further, possibly due to random distribution effects. When the carrier density is increased further by doping Sb or La, the localization behavior seems to disappear because of the screening effects of the free-electron carriers.

The temperature-dependent mobilities of $Ba(Sn,Sb)O_3$ show relatively small variations less than 20%, as seen in Fig. 5(b), while those of $(Ba,La)SnO_3$ reported in a previous work[23] show about 50% change from 2 to 300 K. As the carrier densities of $Ba(Sn,Sb)O_3$ are almost constant as a function of temperature, the resistivity variation over temperature becomes small accordingly [Fig. 5(c)]. The residual resistivity values for nominal doping levels, i.e., $x = 0.03$, 0.05, and 0.10, are typically found to be about 0.66 mΩ cm ($n = 1.02 \times 10^{20}$ cm^{-3}), 0.81 mΩ cm ($n = 1.11 \times 10^{20}$ cm^{-3}), and 0.77 mΩ cm ($n = 2.15 \times 10^{20}$ cm^{-3}), respectively, while the reported residual resistivity of $(Ba,La)SnO_3$ is around 0.12 mΩ cm at a similar carrier-density level ($n = 0.9 \times 10^{20}$ cm^{-3}; see Ref. 23). At the carrier density of 0.9×10^{20} cm^{-3}(3×10^{20} cm^{-3}), those resistivity values of $Ba(Sn,Sb)O_3$ are at least about five (ten) times larger than that of $(Ba,La)SnO_3$ (see Refs. 22 and 23), implying that the carrier scattering is much stronger in $Ba(Sn,Sb)O_3$.

D. Optical transmission spectra

The transmittance and absorption coefficient (α) spectra of $BaSnO_{3-\delta}$ and $Ba(Sn,Sb)O_3$ single crystals are shown in Figs. 6(a) and 6(b) as a function of photon energy. Transmittance of the $BaSnO_{3-\delta}$ single crystal reaches as high as 0.7 in the visible spectral region (1.8–3.1 eV),[23] while transmittance of $Ba(Sn,Sb)O_3$ is reduced down to 0.2–0.3. Moreover, transmittance is progressively suppressed at a low frequency region, resulting in a Drude-type absorption tail due to the increase of free carriers. It is noted that the steep increase in α around 3 eV has slightly shifted to a higher energy with the increase of the Sb doping, indicating that the optical gap of $Ba(Sn,Sb)O_3$ shifts to a higher energy owing to the Burstein-Moss shift[40,41] as often observed in degenerate semiconductors. The as-grown $Ba(Sn,Sb)O_3$ single crystals seem to be black [Fig. 1(b)]. However, if the crystal is thinned down to less than 100 μm, it indeed becomes transparent, as illustrated in the inset of Fig. 6. If the experimentally determined absorption coefficient in the visible spectral region ($\alpha = 100$–600 cm^{-1}) is used, the transmittance of $Ba(Sn,Sb)O_3$ film with 100-nm thickness is calculated to be ~0.8. Therefore, $Ba(Sn,Sb)O_3$ yet should be another transparent electronic material system.

According to the band calculation in Fig. 3, $BaSnO_3$ has an indirect minimum gap. Consistent with this, our previous experimental study on $BaSnO_3$ (see Ref. 23) confirmed that the optical transitions with the lowest energy have an indirect gap nature. On the other hand, direct optical transitions occurring in a slightly higher energy were quite strong in this material system as similarly observed in a perovskite $SrGeO_3$, a new TCO candidate reported recently.[42] Therefore, to determine the optical gap evolution with doping levels in $Ba(Sn,Sb)O_3$, the direct gap was estimated with the α^2 vs. photon energy curves [Fig. 6(c)]. Estimated direct optical gaps in $BaSnO_{3-\delta}$ and two $Ba(Sn,Sb)O_3$ ($n = 1.21 \times 10^{20}$ and 1.88×10^{20} cm^{-3})

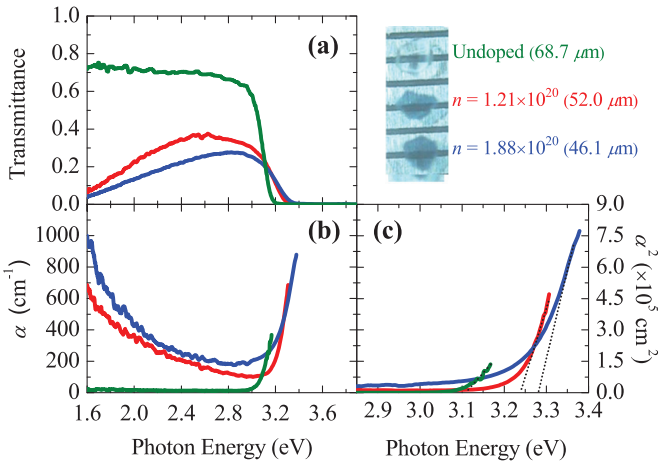

FIG. 6. (Color online) (a) Transmission spectra and (b) absorption coefficient (α) of undoped $BaSnO_{3-\delta}$ (Ref. 23) (green) and Ba(Sn,Sb)O_3 single crystals [$n = 1.21 \times 10^{20}$ cm^{-3} (red) and 1.88×10^{20} cm^{-3} (blue)] are plotted as a function of photon energy. The inset photo image shows undoped $BaSnO_{3-\delta}$ and Ba(Sn,Sb)O_3 single crystals. (c) The curves of α^2 vs. photon energy for both undoped $BaSnO_{3-\delta}$ and Ba(Sn,Sb)O_3 single crystals.

crystals are found to be ~3.10 eV, 3.23 eV, and 3.28 eV, respectively.

Such a systematic optical gap increase directly shows the existence of the Burstein-Moss shift, which in turn renders us to extract the effective mass experimentally.[40,41] According to the Burstein-Moss shift, the difference in the optical band gap (ΔE) between undoped and doped semiconductors is predicted as $\Delta E = h^2(3n/\pi)^{2/3}/(8m^*)$, under the assumption that the conduction band of $BaSnO_3$ has a parabolic dispersion. Here, h is Plank constant, and m^* is effective mass. Figure 7 shows that the resultant ΔE vs. $n^{2/3}$ curves of $BaSnO_3$ and Ba(Sn,Sb)O_3 single crystals are close to being linear, indicating the validity of the parabolic band assumption. Based on the linear slope of ΔE vs. $n^{2/3}$, the effective mass is estimated to be $\sim 0.61m_0$. This value is quite close to that of (Ba,La)SnO_3 $\sim 0.60m_0$, which supports that the effective mass is quite similar with each other mainly because the conduction

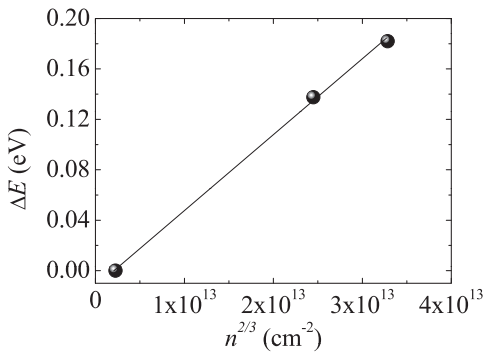

FIG. 7. ΔE is the difference in energy between the optical gaps of the Ba(Sn,Sb)O_3 and $BaSnO_{3-\delta}$ single crystals. ΔE as a function of $n^{2/3}$, showing that the Burstien-Moss shift has a linear dependence. Note that the x-axis ($n^{2/3}$) has a finite offset as the change in the optical gap was referenced to the $BaSnO_{3-\delta}$ crystal where a finite, albeit small, carrier exists due to the oxygen defects.

band shape is quite rigid in the two independently doped $BaSnO_3$ systems.[23] It is noted that the determined value of $\sim 0.61m_0$ is slightly bigger than the theoretically estimated value of $\sim 0.4m_0$ from our LDA calculation and other recent theoretical predictions of 0.06–0.20m_0 (see Refs. 35 and 36).

IV. DISCUSSION

In this section, based on the mobility behavior presented in Fig. 4, we will discuss the implications of the scattering mechanism in (Ba,La)SnO_3 and Ba(Sn,Sb)O_3 systems. The electrical mobility (μ) is defined as

$$\mu = e\tau/m^*, \tag{1}$$

where e is the electron charge and τ is the carrier-scattering time. In general, when multiple scattering sources exist, the scattering rates of individual sources should contribute to determine a total scattering rate. The carrier-scattering rate τ^{-1} becomes momentum-independent when the energies of the occupied electron states are isotropic and depend only upon the magnitude of the momentum when spherically symmetric scattering potential exits. In the momentum-independent approximation as well as in a weak scattering limit,[43] the total electron scattering rate can rather be simply calculated as a sum of several scattering rates according to the Matthiessen's rule:

$$\tau^{-1} = \sum \tau_i^{-1}, \tag{2}$$

where τ_i^{-1} is the electron scattering rate from the ith scattering source. Similarly, the total electrical mobility should be also determined by the mobility for the ith scattering source μ_i:

$$\mu^{-1} = \sum \mu_i^{-1}. \tag{3}$$

There are many sources for carrier scattering, e.g., phonons, ionized impurities, neutral impurities, grain boundaries, crystallographic defects (stacking faults and dislocations), etc. Among these, the crystallographic defects might be negligible in this case because the grown single crystals seem to show high quality. When the rocking curves were measured in the (002) reflection via the so-called ω scan, both (Ba,La)SnO_3 and Ba(Sn,Sb)O_3 single crystals showed quite small and similar full-width at half-maximum values (0.03–0.04°). This observation suggests that both kinds of single crystals have a high degree of crystallinity, and the crystalline defects, if any, are comparable each other. Therefore, we conclude that the scattering from crystallographic defects are presumably minimized or at least comparable in (Ba,La)SnO_3 and Ba(Sn,Sb)O_3.

For doped $BaSnO_{3-\delta}$, Ba(Sn,Sb)O_3, and (Ba,La)SnO_3 single crystals, one of the main sources of electron scattering is likely to be the ionized-dopant scattering, as they all contain Sb^{5+}, La^{3+} ions, or oxygen vacancy V_O. All the single crystals investigated in this work seem to be in the degenerately doped regime as the carrier density is nearly constant over the temperature variation. Moreover, the conduction band of $BaSnO_3$ has nearly a parabolic dispersion at around the Γ-point, as shown in Fig. 3. The linear dependence in the ΔE vs. $n^{2/3}$ plot also suggests that the conduction band of Ba(Sn,Sb)O_3 single crystals should be close to the parabolic

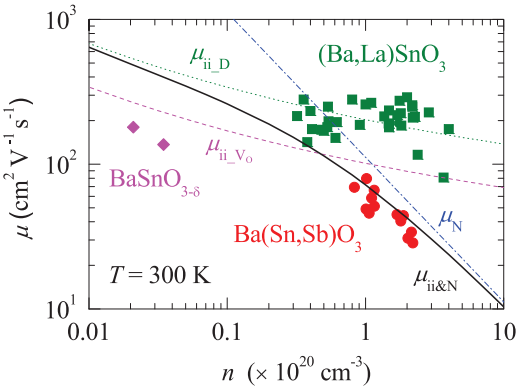

FIG. 8. (Color online) Closed squares (red) and circles (green) and diamonds (violet) are for the mobility vs. carrier density data of $Ba(Sn,Sb)O_3$, $(Ba,La)SnO_3$, and $BaSnO_{3-\delta}$ single crystals, respectively. The dotted line (green) and dashed line (violet) are the theoretically estimated mobility governed by the ionized dopants (La or Sb) (μ_{ii_D}) and the oxygen vacancies ($\mu_{ii\_V_O}$), respectively. The dashed-dotted line (blue) shows the estimated mobility governed by the neutral impurities (μ_N) assuming Sb^{4+}-like neutral impurity sources ($a_B = 0.069$ nm). The solid line (black) shows the total mobility governed by both ionized dopants and neutral impurities ($\mu_{ii\&N}$).

shape. In this limit, the electrical mobility coming from the ionized impurity scattering (μ_{ii}) is expressed by[44,45]

$$\mu_{ii} = \frac{3(\varepsilon_r\varepsilon_0)^2 h^3}{Z^2 m^{*2} e^3}\frac{n}{N_i}\frac{1}{F_{ii}(\xi_d)} \quad \text{with}$$
$$\xi_d = (3\pi^2)^{1/3}\frac{\varepsilon_r\varepsilon_0 h^2 n^{1/3}}{m^* e^2}. \tag{4}$$

Here, the screening function $F_{ii}(\xi_d)$ is given by

$$F_{ii}(\xi_d) = \ln(1+\xi_d) - \frac{\xi_d}{1+\xi_d}, \tag{5}$$

where h is Planck's constant, N_i is the number of ionized dopant per unit volume, ε_r is the dielectric constant, and Z is the effective charge of the ionized impurity (i.e., $Z = +1$ for La^{3+} and Sb^{5+}, and $Z = +2$ for V_O).

The theoretical μ_{ii} expressed in Eqs. (4) and (5) can be calculated for both La- and Sb-doped $BaSnO_3$ as well as $BaSnO_{3-\delta}$ crystals by use of the main experimental parameters $m^* = 0.6m_0$ and $\varepsilon_r = 20$ (Ref. 46). Figure 8 shows the results for the calculated μ_{ii} for the three kind of ionized impurities, i.e., μ_{ii_D} for La or Sb dopants (dotted green line) and $\mu_{ii\_V_O}$ for V_O (dashed violet line). In this calculation, it is assumed that doped ionized impurity has been fully activated, i.e., $n = N_i$ for μ_{ii_D} and $n = 2N_i$ for $\mu_{ii\_V_O}$. If the ionized impurity is less activated, the actual carrier density can be lowered so that the actual mobility predictions can be reduced. Even with this caveat, it is surprising to find that the resultant theoretical mobility values match relatively well with the experimental mobility data in the $BaSnO_{3-\delta}$ and $(Ba,La)SnO_3$ (Fig. 8). In detail, for $BaSnO_{3-\delta}$ single crystals, the predicted mobility value well explains the experimental value, suggesting that the carrier scattering is mainly determined by the inherent impurity scattering coming from V_O. In the case of $(Ba,La)SnO_3$, the μ_{ii_D} curve seems to reproduce the magnitude and the slow evolution of mobility over the carrier-density variation in the range of $n = 1.0\times10^{19}$–4.0×10^{20} cm^{-3}. These observations indicate that ionized impurity scattering is dominant in $(Ba,La)SnO_3$ while additional scattering sources might also exist. It should be noted that the theoretical estimate of the $(Ba,La)SnO_3$ mobility could become further lowered when we condider the contribution of electron-phonon scattering. This implies that the actual strength of the ionized impurity scattering might be smaller than the theoretical prediction, possibly due to the smaller scattering cross section of the La dopants, which are located away from the main conduction paths of SnO_6 octahedral networks.

In sharp contrast, the mobility data of $Ba(Sn,Sb)O_3$ (solid red circles) are clearly deviated from the μ_{ii_D} curve and decrease with the carrier density increase much more steeply than the μ_{ii_D} curve. This directly suggests that the ionized impurity scattering is not a dominant scattering source in $Ba(Sn,Sb)O_3$ as compared with $(Ba,La)SnO_3$, at least in the doping range of $n = 1.0\times10^{19}$–4.0×10^{20} cm^{-3}. As discussed in Sec. III C, the measured n in $Ba(Sn,Sb)O_3$ crystals constitutes only half of the free carrier density expected from the dopant amount, indicating that at least half of the Sb dopants form a bound state of $Sb^{5+}+e^-$ or a Sb-O defect complex, which in turn would behave effectively as Sb^{4+} or neutral impurity in the carrier-scattering process. This result naturally suggests us to consider the possible existence of neutral impurity scattering effects uniquely in $Ba(Sn,Sb)O_3$.

In conventional semiconductors (e.g., Si or Ge) and semiconductor compounds (e.g., GaAs), the neutral impurity scattering governed by the hydrogenlike bound state is usually small at room temperature because the bound state can be easily broken by the thermal energy. For example, the ionization energy (E_i) of the boundstate is ~45 meV for Si and ~10 meV for Ge.[47] Even in the archetypical oxide semiconductors such as In_2O_3, SnO_2, and ZnO, the E_i values, proportional to $m^*/{\varepsilon_r}^2$ (see Ref. 47) are estimated to be similarly small; their ε_r values of 8–14 (Ref. 44) are comparable to those of Si (11.7) and Ge (15.8), and their m^* values [$0.24m_0$–$0.4m_0$ (see Refs. 31–33)] are also similar to those of Si (~$0.1\,m_0$) and Ge (~$0.2\,m_0$).[47] In $BaSnO_3$ with $\varepsilon_r = 20$ (see Ref. 46), the value of E_i is expected be even smaller than those of typical oxdie semicondutors. Therefore, the conventional hydrogenlike bound state is not likely the main source of neutral impurity scattering in the electron-doped $BaSnO_3$. In the case of $Ba(Sn,Sb)O_3$, however, we postulate that the Sb^{4+}-like neutral site can be quite stable even at room temperature because it can be formed either by the mixed-valent character of the Sb ions or by the defect complexes composed of Sb dopants and interstitial oxygen. In both cases, the density of those neutral impurities can be comparable to the density of Sb ions, possibly leading to strong neutral impurity scattering in $Ba(Sn,Sb)O_3$.

In conventional semiconductors, the effective mobility due to the neutral impurities μ_N is likely to be expressed as[48]

$$\mu_N = \frac{2\pi e}{10 a_B h}\frac{1}{N_N} \quad \text{with} \quad a_B = \frac{\varepsilon_r\varepsilon_0 h^2}{\pi m^* e^2}, \tag{6}$$

where N_N is the number of neutral impurities per unit volume and a_B is the scaled Bohr radius of a hydrogenlike bound state. As the inactive free carrier density in $BaSn_{1-x}Sb_xO_3$ ($x = 0.03$,

0.05, and 0.10) single crystals was roughly proportional to the actual carrier density, keeping their ratio of ~50%, it is natural to assume that N_N is equal to the carrier density (n). Then, Eq. (6) predicts that the carrier scattering from the neutral impuritylike sources is proportional to n. The experimental mobility data vs. n curve in Ba(Sn,Sb)O_3 (Fig. 8) is indeed roughly proportional to n^{-1} so that the neutral impurity scattering model seems to well explain the n dependence of the mobility.

On the other hand, upon applying strictly Eq. (6) ($\varepsilon_r = 20$), the calculated mobility is found to be less than 10 cm^2 V^{-1} s^{-1} at $n = 1 \times 10^{20}$ cm^{-3}, being much smaller than the experimental data. Therefore, it is likely that the a_B, an atomic radius of the hydrogenlike scattering source composed of a donor ion and a free electron, is overestimated in our case and should remain as an unknown parameter. Assuming that the neutral impurity in this case might be close to the state of Sb^{4+}, we apply $a_B = 0.069$ nm as the ionic radius of the Sb^{4+} ion. The value was estimated from the average radius of those Sb^{3+} and Sb^{5+} ions as the ionic radius of the Sb^{4+} is unknown. The resultant mobility curve μ_N based on these assumptions is shown as a dotted-dashed line (blue) in Fig. 8. Although it is an empirical attempt, the estimated mobility values of the Ba(Sn,Sb)O_3 seem to roughly match with the experimental data, suggesting the presence of the neutral impurity scattering coming from a bound state close to the Sb^{4+}-like ions. In real materials, it is expected that Ba(Sn,Sb)O_3 should have the scattering contributions from the both neutral and ionized impurities. Thus, the predicted mobility curve for Ba(Sn,Sb)O_3 might be close to the curve of $\mu_{ii\&N}$ (solid black line), which is the total mobility governed by both ionized dopants and neutral impurities.

In sharp contrast to the case of Ba(Sn,Sb)O_3, the additional contribution from the neutral impurity scattering does not seem to exist or can be at least negligible in (Ba,La)SnO_3. As pointed out in previous reports,[22,23] one of main differences between (Ba,La)SnO_3 and Ba(Sn,Sb)O_3 systems is the location of dopants. The reduced mobility of Ba(Sn,Sb)O_3 seems to be closely associated with the position of the Sb dopants in the middle of the conduction path, i.e., SnO_6 octahedra, which is likely to facilitate the neutral impurity scattering in Ba(Sn,Sb)O_3. It should be finally pointed out that the electron-phonon scattering might not be negligible at 300 K. Although the electron-phonon scattering can be almost independent of carrier density, its inclusion will certainly reduce the predicted total mobility further to better match with the experimental data.

V. CONCLUSIONS

In summary, we succeeded in growing high quality Ba(Sn,Sb)O_3 single crystals and found that they are n-type semiconductors in a degenerate doping regime. The highest mobility at 300 K was found to be 79.4 cm^2 V^{-1} s^{-1} in a carrier density of 1.02×10^{20} cm^{-3}. Measurements of the transmission spectra suggest that Ba(Sn,Sb)O_3 can become transparent in a thin-film form and predict the effective mass of ~$0.6m_0$ based on the Burstein-Moss shift. It is newly found in the Ba(Sn,Sb)O_3 system that the experimental mobility data at 300 K shows rather a steep decrease with carrier density increase, being roughly proportional to n^{-1} and becomes smaller than those of (Ba,La)SnO_3 by a factor of ~5–10 in the doping range of $n = 0.9 \times 10^{19} - 3.0 \times 10^{20}$ cm^{-3}. Based on the mobility behavior, it is argued that the electron scattering due to the neutral impurity scattering exists significantly in the Ba(Sn,Sb)O_3 system in addition to the ionized dopant scattering, while the latter seems to be dominant in the (Ba,La)SnO_3 system. The presence of Sb dopants in the middle of the conduction paths of SnO_6 octahedral network is attributed to the increase of free carrier-trapping effect and the resultant enhancement of neutral impurity scattering. Our study implies that the Ba-site doping is more effective than the Sn-site doping to realize the high electrical mobility in the electron-doped $BaSnO_3$ system.

ACKNOWLEDGMENTS

We thank Kookrin Char for helpful discussions and Won Hee Cho for careful readings. We acknowledge support from the NRF through Creative Research Initiative (2010-0018300) and the MKE through the Fundamental R&D program for Core Technology of Materials. This work was also supported by the Institute for Basic Science (IBS) in Korea and the New & Renewable Energy Technology Development Program of the Korea Institute of Energy Technology Evaluation and Planning (2011T100100318) funded by the Ministry of Knowledge Economy.

*Corresponding author: khkim@phya.snu.ac.kr

[1] D. S. Ginley and C. Bright, MRS Bull. **25**, 15 (2000).
[2] A. J. Freeman, K. R. Poeppelmeier, T. O. Mason, R. P. H. Chang, and T. J. Marks, MRS Bull. **25**, 45 (2000).
[3] T. Minami, MRS Bull. **25**, 38 (2000).
[4] H. Hosono, Thin Solid Films **515**, 6000 (2007).
[5] Z. K. Tang, G. K. L. Wong, P. Yu, M. Kawasaki, A. Ohtomo, H. Koinuma, and Y. Segawa, Appl. Phys. Lett. **72**, 3270 (1998).
[6] H. Ohta, M. Orita, M. Hirano, H. Tanji, H. Kawazoe, and H. Hosono, Appl. Phys. Lett. **76**, 2740 (2000).
[7] T. Makino, Y. Segawa, A. Tsukazaki, A. Ohtomo, and M. Kawasaki, Appl. Phys. Lett. **87**, 022101 (2005).
[8] K. Nomura, H. Ohta, K. Ueda, T. Kamiya, M. Hirano, and H. Hosono, Science **300**, 1269 (2003).
[9] H.-H. Wang, D.-F. Cui, S.-Y. Dai, H.-B. Lu, Y.-L. Zhou, Z.-H. Chen, and G.-Z. Yang, J. Appl. Phys. **90**, 4664 (2001).
[10] J. H. Cho and H. J. Cho, Appl. Phys. Lett. **79**, 1426 (2001).
[11] R. P. Wang and C. J. Tao, J. Cryst. Growth **245**, 63 (2002).
[12] B. Hadjarab, A. Bouguelia, and M. Trari, J. Phys. Chem. Solids **68**, 1491 (2007).
[13] P. Singh, D. Kumar, and O. Parkash, J. Appl. Phys. **97**, 074103 (2005).
[14] U. Lampe, J. Gerblinger, and H. Meixner, Sens. Actuators, B **24–25**, 657 (1995).

[15]H. Mizoguchi, H. W. Eng, and P. M. Woodward, Inorg. Chem. **43**, 1667 (2004).
[16]R. J. Cava, P. Gammel, B. Batlogg, J. J. Krajewski, W. F. Peck, Jr., L. W. Rupp, Jr., R. Felder, and R. B. van Dover, Phys. Rev. B **42**, 4815 (1990).
[17]R. Claessen, M. G. Smith, J. B. Goodenough, and J. W. Allen, Phys. Rev. B **47**, 1788 (1993).
[18]T. Huang, T. Nakamura, M. Itoh, Y. Inaguma, and O. Ishiyama, J. Mater. Sci. **30**, 1556 (1995).
[19]M. Yasukawa, T. Kono, K. Ueda, H. Yanagi, and H. Hosono, Mater. Sci. Eng. B **173**, 29 (2010).
[20]H. F. Wang, Q. Z. Liu, F. Chen, G. Y. Gao, W. Wu, and X. H. Chen, J. Appl. Phys. **101**, 106105 (2007).
[21]Q. Liu, J. Dai, Z. Liu, X. Zhang, G. Zhu, and G. Ding, J. Phys. D **43**, 455401 (2010).
[22]H. J. Kim, U. Kim, H. M. Kim, T. H. Kim, H. S. Mun, B.-G. Jeon, K. T. Hong, W.-J. Lee, C. Ju, K. H. Kim, and K. Char, Appl. Phys. Express **5**, 061102 (2012).
[23]H. J. Kim, U. Kim, T. H. Kim, J. Kim, H. M. Kim, B.-G. Jeon, W.-J. Lee, H. S. Mun, K. T. Hong, J. Yu, K. Char, and K. H. Kim, Phys. Rev. B **86**, 165205 (2012).
[24]X. Luo, Y. S. Oh, A. Sirenko, P. Gao, T. A. Tyson, K. Char, and S.-W. Cheong, Appl. Phys. Lett. **100**, 172112 (2012).
[25]A. Ohtomo and H. Y. Hwang, Nature **427**, 423 (2004).
[26]T. Kolodiazhnyi, A. Petric, M. Niewczas, C. Bridges, A. Safa-Sefat, and J. E. Greedan, Phys. Rev. B **68**, 085205 (2003).
[27]K. Ueda, H. Yanagi, H. Hosono, and H. Kawazoe, Phys. Rev. B **56**, 12998 (1997).
[28]G. Kresse and J. Furthmüller, Phys. Rev. B **54**, 11169 (1996).
[29]P. E. Blöchl, Phys. Rev. B **50**, 17953 (1994).
[30]D. M. Ceperley and B. J. Alder, Phys. Rev. Lett. **45**, 566 (1980).
[31]H. Odaka, S. Iwata, N. Taga, S. Ohnishi, Y. Kaneta, and Y. Shigesato, Jpn. J. Appl. Phys. **36**, 5551 (1997).
[32]P. D. Borges, L. M. R. Scolfaro, H. W. L. Alves, and E. F. da Silva, Jr., Theor. Chem. Acc. **126**, 39 (2010).
[33]M. Oshikiri, Y. Imanaka, F. Aryasetiawan, and G. Kido, Physica B **298**, 472 (2001).
[34]W. Wunderlich, H. Ohta, and K. Koumoto, Physica B **404**, 2202 (2009).
[35]E. Moreira, J. M. Henriques, D. L. Azevedo, E. W. S. Caetano, V. N. Freire, U. L. Fulco, and E. L. Albuquerque, J. Appl. Phys. **112**, 043703 (2012).
[36]H.-R. Liu, J.-H. Yang, H. J. Xiang, X. G. Gong, and S.-H. Wei, Appl. Phys. Lett. **102**, 112109 (2013).
[37]Y. Shigesato and David C. Paine, Appl. Phys. Lett. **62**, 1268 (1993).
[38]P. Erhart and K. Albe, J. Appl. Phys. **102**, 084111 (2007).
[39]Y. Z. Wang, E. Bevillon, A. Chesnaud, G. Geneste, and G. Dezanneau, J. Phys. Chem. C. **113**, 20486 (2009).
[40]E. Burstein, Phys, Rev. **93**, 632 (1954).
[41]T. S. Moss, Proc. Phys. Soc. (London) B **67**, 775 (1954).
[42]H. Mizoguchi, T. Kamiya, S. Matsuishi, and H. Hosono, Nature Comm. **2**, 470 (2011).
[43]M. P. Marder, *Condensed Matter Physics*, 2nd ed. (Wiley, New York, 2010), pp. 523–529.
[44]K. Ellmer, J. Phys. D **34**, 3097 (2001).
[45]R. B. Dingle, Philos. Mag. **46**, 831 (1955).
[46]P. Singh, B. J. Brandenburg, C. P. Sebastian, P. Singh, S. Singh, D. Kumar, and O. Parkash, Jpn. J. Appl. Phys. **47**, 3540 (2008).
[47]C. Kittel, *Introduction to Solid State Physics*, 7th ed. (Wiley, New York, 1996), pp. 221–225.
[48]C. Erginsoy, Phys. Rev. **79**, 1013 (1950).